applied optics

Simplified Phase Diversity algorithm based on a first-order Taylor expansion

DONG ZHANG,[1,2,*] XIAOBIN ZHANG,[1,2] SHUYAN XU,[1] NANNAN LIU,[1] AND LUOXIN ZHAO[1]

[1]Space Optics Department, Changchun Institute of Optics, Fine Mechanics and Physics, Chinese Academy of Sciences, Changchun, Jilin 130033, China
[2]University of Chinese Academy of Sciences, Beijing 100049, China
*Corresponding author: zd815955486@icloud.com

Received 4 May 2016; revised 11 August 2016; accepted 11 August 2016; posted 2 September 2016 (Doc. ID 264508); published 26 September 2016

We present a simplified solution to phase diversity when the observed object is a point source. It utilizes an iterative linearization of the point spread function (PSF) at two or more diverse planes by first-order Taylor expansion to reconstruct the initial wavefront. To enhance the influence of the PSF in the defocal plane which is usually very dim compared to that in the focal plane, we build a new model with the Tikhonov regularization function. The new model cannot only increase the computational speed, but also reduce the influence of the noise. By using the PSFs obtained from Zemax, we reconstruct the wavefront of the Hubble Space Telescope (HST) at the edge of the field of view (FOV) when the telescope is in either the nominal state or the misaligned state. We also set up an experiment, which consists of an imaging system and a deformable mirror, to validate the correctness of the presented model. The result shows that the new model can improve the computational speed with high wavefront detection accuracy.

OCIS codes: (070.2025) Discrete optical signal processing; (100.5070) Phase retrieval; (110.1080) Active or adaptive optics.

http://dx.doi.org/10.1364/AO.55.007872

1. INTRODUCTION

In the process of assembly, transportation, and launch, the position and surface of the optical components may have changes due to vibration and other environmental factors, which is called misalignment and will result in decrease of the image quality [1]. By introducing the active optics, the misalignment can be corrected to some extent. Active optical technology mainly includes three parts [2]: first, detecting the wavefront of the misaligned system; second, solving the misalignments using the detected wavefront; last, correcting the misalignments. Many methods have been proposed to detect the wavefront of the system. These methods can be classified into two types: one depends on the hardware facilities such as Shack–Hartmann [3], Curvature Sensing [4] and Pyramid Sensor [5]; the other uses images such as Phase Retrieval (PR) [6] and Phase Diversity (PD) [7]. Phase Diversity only needs two images to detect the wavefront, thus the structure is quite simple and easy to implement. However, because of the complex relationship between the phase and the objective function of the conventional algorithm, it is quite difficult to solve the phase directly. Researchers often use nonlinear optimization algorithms to solve the objective function, thus the calculation is quite complicated, and the real-time performance is very poor. This results in PD often being used for image reconstruction. The calculated amount of PD algorithm is the main restriction for the application of PD in active optics. Keller *et al.* [8,9] proposed a first-order and second-order approximation method to expand the generalized pupil function (GPF), which can separate the point spread function (PSF) into its odd and even parts. By analyzing the PSFs of the focal and defocal planes, they acquire the relationship between the phase and the even part of the PSF in both the focal and defocal planes, thereby reducing the computational complexity. Smith *et al.* [10–13] process a first-order and second-order Taylor expansion to the PSF at zero phase each time to obtain a set of approximation solutions of the true phase, and then gradually correct the optical system by deforming the mirror until the phase approaches zero. Because the Taylor expansion coefficients of PSF at zero phase can be obtained in advance, it can greatly reduce the calculation time. However, it is complex to use a deformable mirror system to iteratively reduce the aberrations in the practical application of active optics (especially when it is used on the space telescope). Besides, the central energy of the PSF in the defocal plane is usually very low compared to the focal plane, so the influence of the PSF in the defocal plane on the calculated result is much weaker than that of the focal PSF, which will easily lead to a large error in the result. In this paper, we utilize a first-order Taylor expansion of the PSF to establish a new objective function, which can strengthen the influence of the PSF in the defocal plane and can be easily solved. By making the expansion at the point where we get in the last iteration, we can acquire the aberration coefficients directly without the iterative correction by a deformable mirror.

2. TRADITIONAL PHASE DIVERSITY ALGORITHM

The image of the optical system can be approximated by the following convolution:

$$i(u,\nu) = \mathrm{psf}(u,\nu) * o(u,\nu), \tag{1}$$

where $o(u,\nu)$ is the observed object, and $\mathrm{psf}(u,\nu)$ is the PSF of the optical system. (u,ν) is the coordinate vector in the pupil plane.

The relationship between the phase φ and the intensity distribution in the image plane of a PSF can be described using the Fourier transformation of the GPF as

$$\mathrm{psf}(u,v,\varphi) = |f\{P(u,v,\varphi)\}|^2, \tag{2}$$

$f\{\bullet\}$ means the Fourier transform.

The GPF is defined as

$$P(u,v,\varphi) = A(u,v)e^{i\varphi(u,v,\alpha)}, \tag{3}$$

where $A(u,v)$ is the pupil function (1 over the pupil and 0 in the exterior), and the phase can be approximated using a normalized Zernike basis:

$$\varphi(u_j,v_j,\alpha) = Z(u_j,v_j)^T \cdot \alpha. \tag{4}$$

As for the other image, of which the diversities are usually acquired by defocus, the phase is:

$$\varphi_d(u_j,v_j,\alpha) = Z(u_j,v_j)^T \cdot (\alpha+\beta), \tag{5}$$

where β is the known diversity.

Paxman [14] has deduced a likelihood function to evaluate the similarity between the phase and the image:

$$L(\alpha) = -\sum_{u,\nu\in\chi} \frac{|D_1(u,\nu)S_2(u,\nu) - D_2(u,\nu)S_1(u,\nu)|}{|S_1(u,\nu)|^2 + |S_2(u,\nu)|^2}, \tag{6}$$

where $D_k(u,\nu)|_{k=1,2}$ is the discrete Fourier transform of the focal/defocal image, and $S_k(u,\nu)|_{k=1,2}$ is the optical transfer function (OTF) of the focal/defocal plane. We treat the object, the PSFs, and the images as periodic arrays with a period cell of size $N \times N$. There arrays are completely specified by their functional values on the set χ, where $\chi = \{0,1,\cdots,N-1\} \times \{0,1,\cdots,N-1\}$[14].

When the function arrives at its minimum, we will acquire the phase of the optical system.

3. LINEAR APPROXIMATION OF PSF BASED ON TAYLOR EXPANSION

The relationship between Eq. (6) and the phase is very complex, so it is usually very difficult to find its minimum. Researchers often use Broyden–Fletcher–Goldfarb–Shanno (BFGS) method to solve the function [15]. But the conventional BFGS method only converges to global optima when the cost function is convex, and it usually costs too much time.

When the observed object is a point source, we can approximate the PSF by first-order Taylor expansion in $\alpha = 0$:

$$\mathrm{psf}(\alpha) = h_0 + h_1 \cdot \alpha + O\|\alpha\|^2, \tag{7}$$

where $h_0 = \mathrm{psf}(\alpha)|_{\alpha=0}$, $h_1 = \frac{\partial \mathrm{psf}(\alpha)}{\partial\alpha}|_{\alpha=0}$, and $O\|\alpha\|^2$ is the 2nd-order Lagrange residue.

When the phase is very small, the 2nd-order Lagrange residue can be ignored. Thus, the PSFs of the focal and defocal planes can be written as

$$\begin{aligned} \mathrm{psf}_f(\alpha) &= h_{0,f} + h_{1,f}\cdot\alpha \\ \mathrm{psf}_d(\alpha) &= h_{0,d} + h_{1,d}\cdot\alpha. \end{aligned} \tag{8}$$

So the difference between the real PSFs of the image plane and the PSFs that we rebuilt is:

$$E = (\|\mathrm{psf}_f(\alpha) - i_f\|_2^2 + k\|\mathrm{psf}_d(\alpha) - i_d\|_2^2)_{\min},$$

i.e.,

$$E = (\|h_{1,f}\alpha + h_{0,f} - i_f\|_2^2 + k\|h_{1,d}\alpha + h_{0,d} - i_d\|_2^2)_{\min}, \tag{9}$$

k is used to balance the impact of the focal image and the defocal image. Usually $k = \frac{\|h_{1,f}\alpha+h_{0,f}-i_f\|_2^2}{\|h_{1,d}\alpha+h_{0,d}-i_d\|_2^2}$.

If we take $\frac{\partial E}{\partial\alpha} = 0$, we will get:

$$U_1^T U_1\alpha - U_1^T W_1 + k^2 U_2^T U_2\alpha - k^2 U_2^T W_2 = 0,$$

i.e.,

$$\alpha = (U_1^T U_1 + k^2 U_2^T U_2)^{-1}(U_1^T W_1 + k^2 U_2^T W_2), \tag{10}$$

where $U_1 = h_{1,f}$, $U_2 = h_{1,d}$, $W_f = i_f - h_{0,f}$, $W_d = i_d - h_{0,d}$.

Usually, the accuracy of the first-order Taylor expansion in $\alpha = 0$ is not enough. So we make the expansion at the point where we get in the last iteration. Equation (8) will be rewritten as

$$\begin{aligned} \mathrm{psf}_f(\alpha) &= h_{0,f,k} + h_{1,f,k}\cdot(\alpha-\alpha_k) \\ \mathrm{psf}_d(\alpha) &= h_{0,d,k} + h_{1,d,k}\cdot(\alpha-\alpha_k), \end{aligned} \tag{11}$$

where $h_{0,f,k} = \mathrm{psf}_f(\alpha)|_{\alpha=\alpha_k}$, $h_{0,d,k} = \mathrm{psf}_d(\alpha)|_{\alpha=\alpha_k}$, $h_{1,f,k} = \frac{\partial \mathrm{psf}_f(\alpha)}{\partial\alpha}|_{\alpha=\alpha_k}$, $h_{1,d,k} = \frac{\partial \mathrm{psf}_d(\alpha)}{\partial\alpha}|_{\alpha=\alpha_k}$.

Thus:

$$\alpha_{k+1} = (U_1^T U_1 + k^2 U_2^T U_2)^{-1}(U_1^T W_1 + k^2 U_2^T W_2) + \alpha_k. \tag{12}$$

4. TIKHONOV REGULARIZATION FUNCTION

The main influence of the noise is that it will increase the difference between the actual PSF and the one that we rebuild using linear approximation. Here, we introduce a Tikhonov regularization function of the first order. Equation (9) can be rewritten as

$$E = (\|h_{1,f}\alpha + h_{0,f} - i_f\|_2^2 + k\|h_{1,d}\alpha + h_{0,d} - i_d\|_2^2 + \lambda\|L_i\alpha\|_2^2)_{\min}. \tag{13}$$

L_i is the i-th differential operator and is used to control the smoothness of the solution during the iterative steps. λ is non-negative regularization parameter [15].

Usually we take

$$L_0 = \begin{bmatrix} 1 & & & \\ & 1 & & \\ & & \ddots & \\ & & & 1 \end{bmatrix},$$

and $\lambda = \sigma^2/S$. σ^2 is the variance of the noise, and S is the power spectral density (PSD). The solution of the Eq. (13) is

$$\alpha = (U_1^T U_1 + k^2 U_2^T U_2 + \lambda L_i^T L_i)^{-1}(U_1^T W_1 + k^2 U_2^T W_2). \tag{14}$$

5. NUMERICAL SIMULATION

In this section, we use ZEMAX to acquire the PSFs both in the focal and defocal planes to solve the phase, and then we contrast them with the phase from ZEMAX. The optical system we choose is the Hubble Space Telescope (Fig. 1), whose parameters we can obtain from the ZEMAX object. Because the Hubble Space Telescope is a typical R-C system, the second mirror shades the pupil in the center. Thus, the pupil function $A(u, v)$ will be an annulus (1 in the annulus and 0 in the exterior). But the phase $\varphi(u, v, \alpha)$ can still be expressed on the whole circle because of the orthogonality of the Zernike Fringe Term, which is validated by the result of the numerical simulation.

First, we choose the original system to validate our algorithm, and then we add some misalignments to the system to taint the phase. To reduce the amount of the calculation, the sampling grid we choose on the pupil plane is 32×32, and 64×64 on the image plane, which can satisfy the Nyquist sampling criterion. The exit pupil diameter is 2.4 m, and the F number of the system is 24. The field we choose is (0.08, 0.08 deg). The Gaussian noise power we add is 30 dB both in the focal and defocal planes. The CPU we used is Intel(R) Core(Tm) i7-4790K, and the frequency is 4.00 GHz.

A. Original Optical System

In Fig. 2, we plot the phase expressed by Zernike Fringe Coefficients. The blue term is the standard data from ZEMAX. The red term is acquired by using the new simplified algorithm (adding Tikhonov regularization and enhancing the influence of the PSF in the defocal plane). The green term is acquired neither using Tikhonov regularization function nor enhancing the influence of the PSF in the defocal plane, and the magenta term is the result of using a traditional PD algorithm.

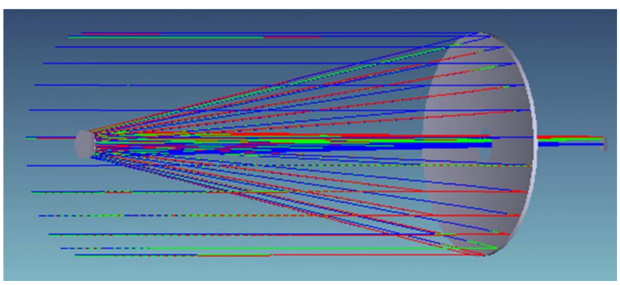

Fig. 1. Sketch map of Hubble Space Telescope (from ZEMAX).

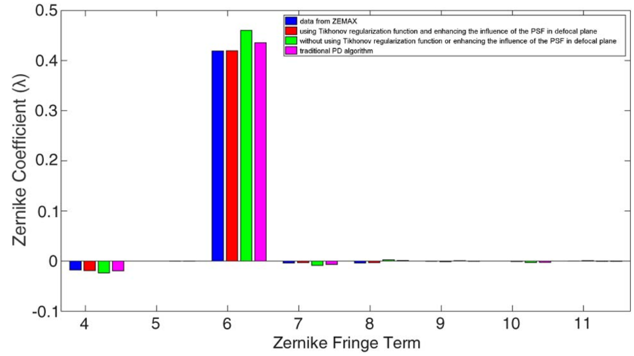

Fig. 2. Phase expressed by Zernike Fringe Coefficients (without misalignments).

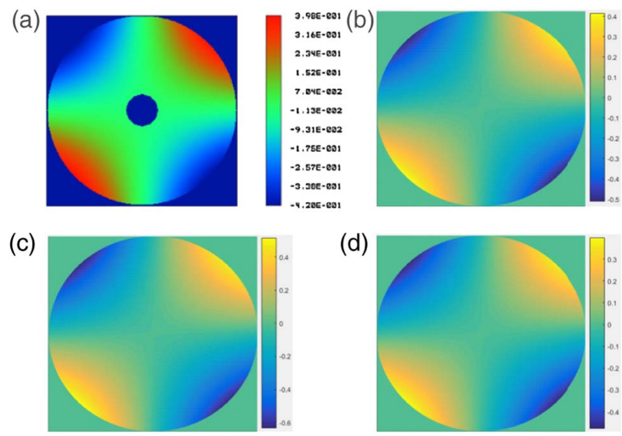

Fig. 3. Wavefront map of HST without misalignments (the unit is λ).

In Fig. 3 we show the wavefront map. Figure 3(a) is the standard map from ZEMAX. Figure 3(b) is reconstructed using the result acquired by the new algorithm. Figure 3(c) is the result of neither using the Tikhonov regularization function nor enhancing the influence of the PSF in the defocal plane, and Fig 3(d) is the result of the traditional PD algorithm.

In Fig. 4 we show the tendency of the RMS between the result and the standard data from ZEMAX during the iteration.

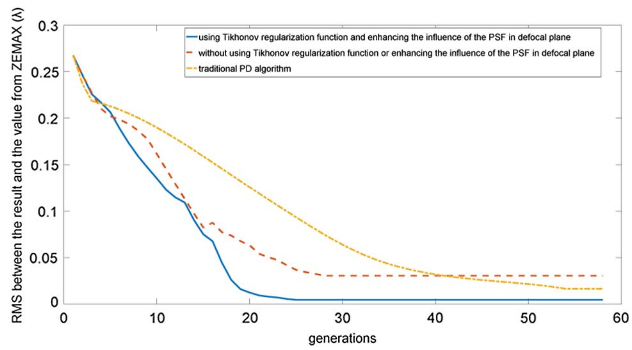

Fig. 4. Tendency of the RMS between the result and the value from ZEMAX during the iteration (without misalignments).

When using the new simplified PD algorithm, the result has the tendency to be stable after the iteration evolves to the 25th generation. The time that the algorithm costs is 1.046 s, and the RMS between the result and the standard data from ZEMAX is 0.0046λ. Without using Tikhonov regularization function or enhancing the influence of the PSF in the defocal plane, the result will be stable after the 29th generation. The time is 1.537 s, and the RMS is 0.0305λ. As for the traditional PD algorithm, the result needs 57 generations to be stable with the time that it costs is 16.731 s, and the RMS is 0.0164λ.

B. System with Misalignments

In the previous section, the original optical system is an ideal model whose phase is too small. When the telescope is sent to the working orbit, some parts of the optical system would not be on the correct place, and the phase will not be very good. In this section, we add some misalignments to the system to stain the phase. In Fig. 5, we show the result as in Fig. 2, and in Fig. 6, we show the wavefront map as in Fig. 3.

In Fig. 7 we see that when using the new simplified PD algorithm, the result has the tendency to be stable after the 5th generation. The time that the algorithm costs is 0.666 s, and the RMS between the result and the standard data from ZEMAX is 0.0072λ. Without using the Tikhonov regularization function or enhancing the influence of the PSF in the defocal plane, the result will be stable after the 8th generation, with the time that it costs is 1.181 s. The RMS is 0.0357λ. The traditional PD algorithm needs 28 generations to be stable, and the time is 10.545 s. The RMS is 0.0186λ.

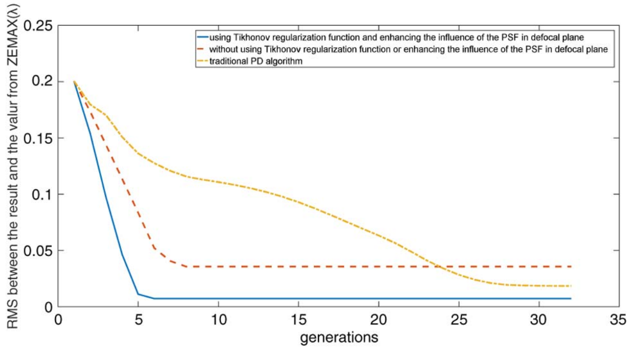

Fig. 7. Tendency of the RMS between the result and the value from ZEMAX during the iteration (with misalignments).

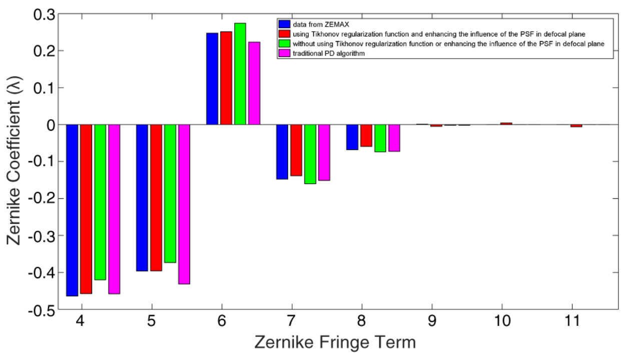

Fig. 5. Phase expressed by Zernike Fringe Coefficients (with misalignments).

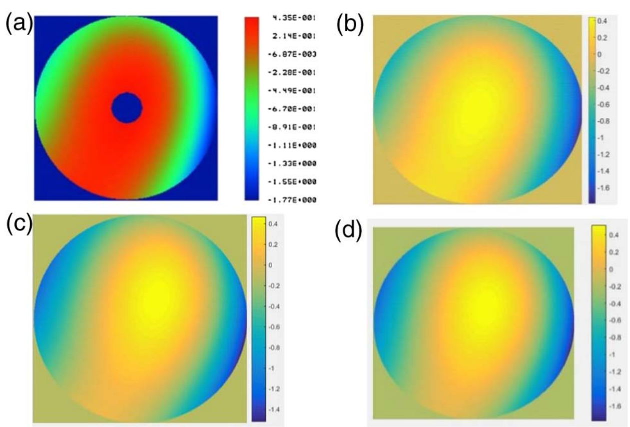

Fig. 6. Wavefront map of HST with misalignments (the unit is λ).

6. EXPERIMENTAL VALIDATION

To validate the algorithm, we use a laser irradiating on a deformable mirror (DM), and then reflecting through some lens. The image is acquired with a CMOS set on the guide rail. Because the Shack–Hartmann method cannot detect the wavefront on the image plane directly, we use the DM to add extra phase. Thus, the Shack–Hartmann can detect the change of the phase. By contrasting the change from Shack–Hartmann with the result that we got from our algorithm, the algorithm will be validated. The focal length is 60 mm, and the F number is 15. The wavelength of the laser is 680 nm. The sketch map and the real facility of the optical system are shown in Figs. 8 and 9.

Figure 10 shows the images on the focal and defocal planes. Figures 10(a) and 10(b) are acquired by the CMOS. We solve the phase using Figs. 10(a) and 10(b) in three ways. The first time we use the new simplified algorithm, and the reconstructed images are shown in Figs. 10(c) and 10(d). The second time we use the simplified algorithm without using the Tikhonov regularization function or enhancing the influence of the PSF in defocal plane, and the images are shown in

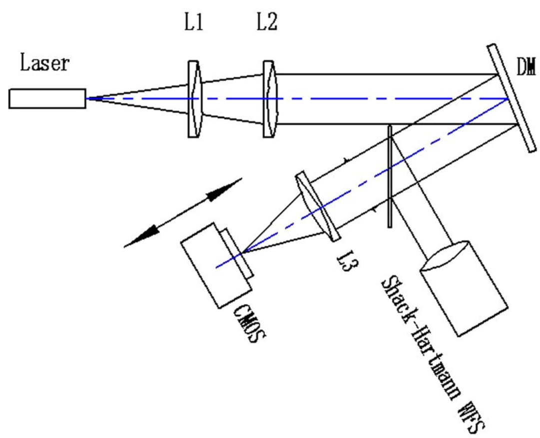

Fig. 8. Sketch map of the optical system used in the experiment.

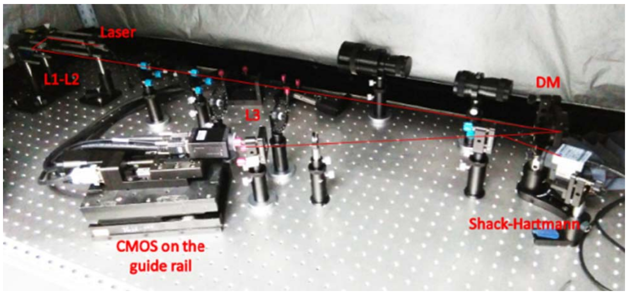

Fig. 9. Snapshot of the experiment.

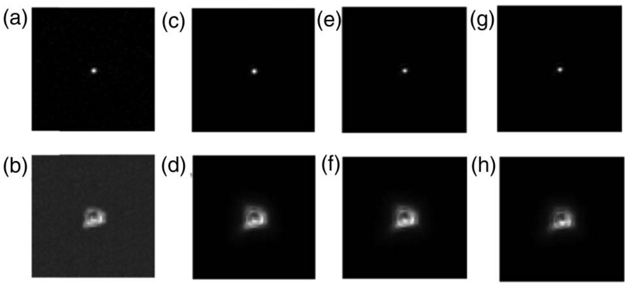

Fig. 10. Images on the focal and defocal planes.

Figs. 10(e) and 10(f). The last time we use the traditional PD algorithm, and the images are shown in Figs. 10(g) and 10(h). To show the defocal image clearly, we divide the image by the maximum of itself. The same operation is performed in Fig. 12.

Figure 11 is the phase of the system by solving Figs. 10(a) and 10(b). The blue term is the result using the Tikhonov regularization function and enhancing the influence of the PSF in the defocal plane. The time that the algorithm costs is 1.16 s. The red term is the result without using the Tikhonov regularization function or enhancing the influence of the PSF in the defocal plane. The time that the algorithm costs is 1.31 s. The green term is the result of the traditional PD algorithm, and the time cost is 18.16 s.

Then, we add some astigmatisms on the DM, and the images on the focal and defocal planes are shown in Figs. 12(a) and 12(b). The reconstructed images on the focal

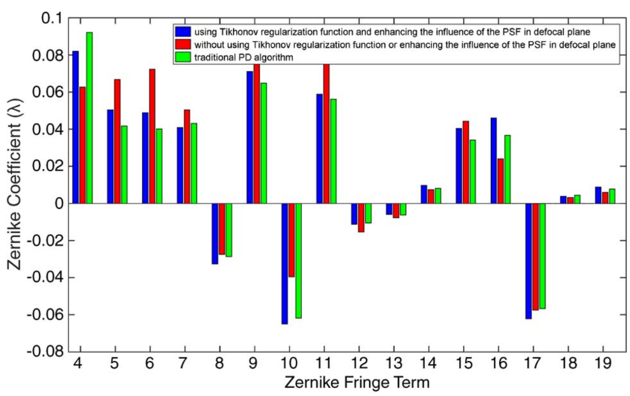

Fig. 11. Phase acquired from the algorithms before adding astigmatisms on the DM.

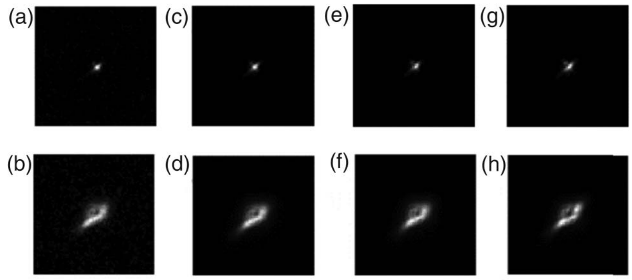

Fig. 12. Images on the focal and defocal planes with some astigmatisms added on the DM.

and defocal planes that in three different ways (using the new simplified algorithm, without using the Tikhonov regularization function or enhancing the influence of the PSF in the defocal plane, and traditional PD algorithm) are shown in Figs. 12(c)–12(h) as Fig. 10.

The results of the three kinds of algorithms are shown in Fig. 13 as Fig. 11. The time that the new algorithm costs is 1.88 s. Without using the Tikhonov regularization function or enhancing the influence of the PSF in the defocal plane, the time is 2.12 s. The traditional PD algorithm costs 23.51 s.

Figure 14 shows the wavefront that the DM added in the system. Figure 14(a) is the output of the Shack–Hartmann. Figure 14(b) is the wavefront reconstructed with the result that was acquired from the new simplified algorithm. Figure 14(c) is reconstructed without using the Tikhonov regularization function or enhancing the influence of the PSF in the defocal plane, and Fig. 14(d) uses the traditional PD algorithm.

The residual error between the wavefront detected by Shack–Hartmann and that reconstructed with the results are shown in Fig. 15. Figure 15(a) shows the difference between the Shack–Hartmann and the new simplified algorithm. Figure 15(b) shows the difference between the Shack–Hartmann and the algorithm without using the Tikhonov regularization function or enhancing the influence of the PSF in the defocal plane. And Fig. 15(c) is the difference between the Shack–Hartmann and the traditional PD algorithm.

We choose the Zernike Fringe Term to fit these residual errors. The results are shown in Fig. 16. The blue term is the result of the new simplified algorithm, with the RMS of 0.0134λ. The red term does not use the Tikhonov regularization

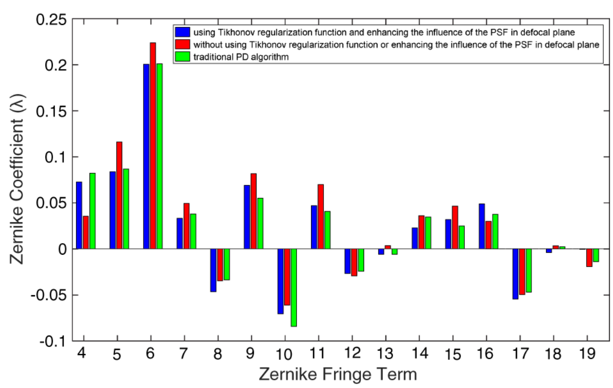

Fig. 13. Phase acquired from the algorithms after adding astigmatisms on the DM.

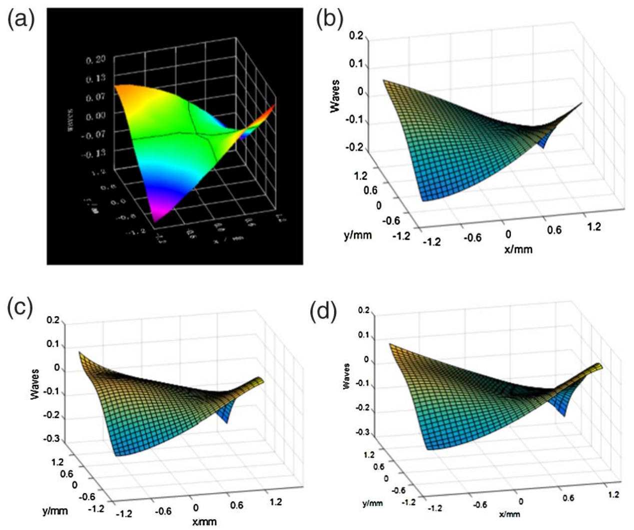

Fig. 14. Wavefront that the DM added in the system: [(a) detected by Shack–Hartmann, (b) using the new simplified algorithm, (c) without using Tikhonov regularization function or enhancing the influence of the PSF in defocal plane, and (d) traditional PD algorithm].

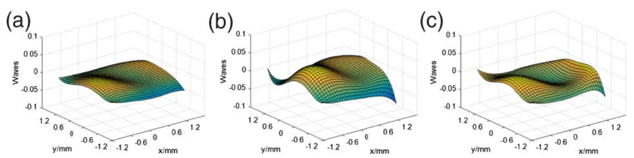

Fig. 15. Residual error between the wavefront from Shack–Hartmann and that reconstructed from the algorithms.

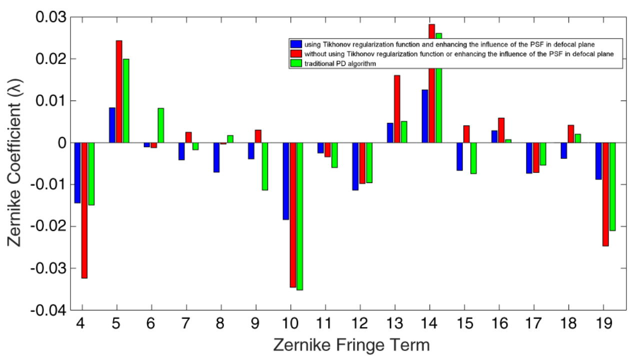

Fig. 16. Differences fitted with Zernike Fringe Term.

function or enhance the influence of the PSF in the defocal plane. The RMS is 0.0277λ. The green term uses the traditional PD algorithm. The RMS is 0.0212λ.

7. CONCLUSION

In this paper, we have presented a simplified PD algorithm based on the first-order Taylor expansion of PSF, when the observed object is a point source. By enhancing the influence of the defocal PSF and introducing the Tikhonov regularization function, the RMS of the result can be approximately 0.01λ according to the numerical simulation and the experiment. The time that the new algorithm costs is about 10% of the traditional PD algorithm.

We solve the wavefront of the Hubble Space Telescope at the edge of FOV with the PSF from ZEMAX, when the telescope is in either the nominal state or the misaligned state. Further on, we set a simple optical system with a DM to change the phase, and use the Shack–Hartmann to detect the change. Both the numerical simulation and the experiment show that the proposed algorithm has a higher accuracy with much faster computation compared to the traditional algorithm.

Funding. National Natural Science Foundation of China (NSFC) (61205143).

REFERENCES

1. C. Qiang, "Wavefront error testing of off-axis three-mirror anastigmatic system using phase diversity technology," Chin. J. Lasers **39**, 1008001 (2012).
2. S. Dingqiang and C. Xiangqun, "Active optics—key technology of the new generation telescopes," Prog. Astron. **17**, 1–17 (1999).
3. H. Hofer, L. Chen, G. Y. Yoon, B. Singer, Y. Yamauchi, and D. R. Williams, "Improvement in retinal image quality with dynamic correction of the eye's aberration," Opt. Express **8**, 631–643 (2001).
4. V. G. Orlov, S. Cuevas, and F. Garfias, *Astronomical Telescopes and Instrumentation* (International Society for Optics and Photonics, 2000), pp. 540–551.
5. I. Iglesias, "Pyramid phase microscopy," Opt. Lett. **36**, 3636–3638 (2011).
6. R. A. Gonsalves, "Phase retrieval and diversity in adaptive optics," Opt. Eng. **21**, 829–832 (1982).
7. M. G. Löfdahl, A. Harwit, K. E. Mitchell, A. L. Duncan, J. H. Seldin, R. G. Paxman, and D. S. Acton, "Phase diversity experiment to measure piston misalignment on the segmented primary mirror of the Keck II telescope," Proc. SPIE **3356**, 190–201 (1998).
8. C. U. Keller, V. Korkiakoski, N. Doelman, R. Fraanje, R. Andrei, and M. Verhaegen, "Extremely fast focal-plane wavefront sensing for extreme adaptive optics," Proc. SPIE **8447**, 844721 (2012).
9. R. A. Gonsalves, "Small-phase solution to the phase-retrieval problem," Opt. Lett. **26**, 684–685 (2001).
10. C. S. Smith, R. Marinica, and M. Verhaegen, "Real-time wavefront reconstruction from intensity measurements," in *3rd AO4ELT Conference: Adaptive Optics for Extremely Large Telescopes* (Arcetri Astrophysical Observatory, 2013).
11. C. S. Smit, R. Marinica, A. J. D. Dekker, M. Verhaegen, V. Korkiakoski, C. U. Keller, and N. Doelman, "Iterative linear focal-plane wavefront correction," J. Opt. Soc. Am. A **30**, 2002–2011 (2013).
12. R. Marinica, C. S. Smith, and M. Verhaegen, "State feedback control with quadratic output for wavefront correction in adaptive optics," in *52nd IEEE Conference on Decision and Control* (Institute for Electrical and Electronic Engineers, 2013), pp. 3475–3480.
13. C. Plantet, S. Meimon, T. Fusco, and J.-M. Conan, "Experimental validation of LIFT for estimation of low-order modes in low-flux wavefront sensing," Opt. Express **21**, 16337–16352 (2013).
14. R. G. Paxman, T. J. Schulz, and J. R. Fienup, "Joint estimation of object and aberrations by using phase diversity," J. Opt. Soc. Am. A **9**, 1072–1085 (1992).
15. Y. Dan, X. Shuyan, and N. Haitao, "Co-phasing of the segmented mirror and image retrieval based on phase diversity using a modified algorithm," Appl. Opt. **54**, 7917–7924 (2015).